

PERTURBATIONS OF SNe Ia LIGHTCURVES, COLORS AND SPECTRAL FEATURES BY CIRCUMSTELLAR DUST

RAHMAN AMANULLAH AND ARIEL GOOBAR

The Oskar Klein Center, Physics Department, Stockholm University, AlbaNova University Center, SE 106 192 Stockholm, Sweden

Draft version January 14, 2013

ABSTRACT

It has been suggested that multiple scattering on circumstellar dust could explain the non-standard reddening observed in the line-of-sight to Type Ia supernovae. In this work we use Monte Carlo simulations to examine how the scattered light would affect the shape of optical lightcurves and spectral features. We find that the effects on the lightcurve widths, apparent time evolution of color excess and blending of spectral features originating at different photospheric velocities should allow for tests of the circumstellar dust hypothesis on a case by case basis. Our simulations also show that for circumstellar shells with radii $r = 10^{16} - 10^{19}$ cm, the lightcurve modifications are well described by the empirical Δm_{15} parameter and intrinsic color variations of order $\sigma_{BV} = 0.05 - 0.1$ arise naturally. For large shell radii an excess lightcurve tail is expected in B band, as observed in e.g. SN 2006X.

Subject headings: dust, extinction — Interstellar medium, nebulae : distance scale — Cosmology : supernovae: general — Stars : supernovae individual SN 2006X — Stars

1. INTRODUCTION

A dramatic breakthrough in cosmology took place more than a decade ago when the accelerated expansion of the universe was discovered through Type Ia supernovae (SNe Ia) used as standardizable candles (Riess et al. 1998; Perlmutter et al. 1999). SNe Ia remain among the best tools to investigate the energy content of the universe, as demonstrated by recent very successful surveys of high- z SNe (Astier et al. 2006; Wood-Vasey et al. 2007; Riess et al. 2007; Kowalski et al. 2008; Kessler et al. 2009; Amanullah et al. 2010). However, the progress for precision cosmology is hampered by systematic uncertainties, notably a potential drift in the SN Ia luminosity and intrinsic colors with cosmic time and the impact of changing dust extinction properties along the line of sight (Nordin et al. 2008). The standardization of SNe Ia generally uses two parameters: the measured color, typically rest-frame $B - V$ and often one more optical color, and an empirically defined lightcurve shape parameter, such as stretch, s (Perlmutter 1997; Guy 2005; Conley et al. 2008), x_1 (Guy et al. 2007), $\Delta m_{15}(B)$ (Phillips 1993; Hamuy et al. 1996) or Δ (Riess et al. 1996; Jha et al. 2007). In this work we examine how multiple scattering of supernova photons on the surrounding material could affect both the lightcurve shapes and colors.

While the reddening of SNe Ia was originally thought to be entirely due to extinction by interstellar dust, there is an increasing body of evidence showing that the measured color excesses to some SN Ia show a steeper wavelength dependence than what is observed for reddened stars in the Milky Way. Likewise, there is no generally accepted model that explains the lightcurve shape variations observed in SNe Ia and its correlations with peak supernova brightness (Phillips 1993).

Following up the work by Wang (2005), Goobar (2008) (hereafter G08) showed that multiple scattering on circumstellar dust could potentially help explaining the low values of the total-to-selective extinction param-

eter, $R_V = A_V/E(B - V) < 3$, observed in the sight lines of near-by Type Ia SNe (Elias-Rosa et al. 2006, 2008; Krisciunas et al. 2007; Wang et al. 2008; Nobili & Goobar 2008).

A Monte Carlo ray tracing technique was used in G08 to investigate the reddening effects in the presence of circumstellar dust and an approximate reddening law for optical and near-IR wavelengths was derived. Folatelli et al. (2010) compared the parametrized model in G08 with high quality $uBgrYJHK$ data from the *Carnegie Supernova Project* and found that it provided particularly good fits for the two most reddened SNe Ia in their sample, SN 2005A and SN 2006X. The success of these comparisons calls for further scrutiny of the model. In this work we investigate the impact of multiple scattering on the shapes of SNe Ia optical lightcurves. We explore how the extra wavelength dependent “random walk” of photons in the presence of scatterers affects the width of broad-band filter lightcurves. In particular, reddened “slow decliners” may be compatible with the scenario in G08.

Furthermore, also the strengths of spectroscopic features as a function of time are likely to be affected, since a varying path-length would lead to a superposition of several SN phases. Throughout the paper we point out how observations could put bounds on the size of a hypothetical circumstellar dust shell.

2. CIRCUMSTELLAR DUST IN THE SINGLE DEGENERATE SCENARIO

In the currently favored Type Ia scenario, a white dwarf accretes mass from a companion star until the Chandrasekhar limit is reached, at which point instabilities lead to an explosion. However, the model requires the accreting white dwarf to expel material accumulating on its surface through fast stellar winds, $v_w \sim 10^2 - 10^3$ km s⁻¹, to avoid the formation of a common envelope between the white dwarf and the donor star which would prevent the explosion (Hachisu et al. 1996; Hachisu & Kato 1999; Hachisu et al. 1999). Con-

densation of dust grains may take place in the ejected matter, possibly also in collisions with the accreting matter. For dust grain growth in stellar winds, the density as a function of distance to the star surface, r , is generically expected to scale as $\rho_{dust} \propto \frac{\dot{M}_w}{v_w r^2}$, where, v_w , is the stellar wind velocity and \dot{M}_w is the mass-loss per unit time, typically of order $10^{-7} M_\odot \text{ yr}^{-1}$ in SNe Ia models.

3. CIRCUMSTELLAR DUST DESTRUCTION BY SN Ia LUMINOSITY

So far, we have assumed that the supernova explosion site is surrounded by dust. However, the radiation from the supernova itself will sublimate dust grains as these are heated up to $T_{sub} \sim 3000$ K. Thus, assuming that the entire UV-optical luminosity of the supernova, is absorbed by surrounding dust grains, we can compute the radius, r_c , where dust grains, if present at the explosion time, would be depleted. From the radiation balance condition:

$$r_c = \left(\frac{L_{bol}(t)}{16\pi\sigma T_{sub} <Q_{IR}>} \right)^{1/2}, \quad (1)$$

where Q_{abs} is the effective absorption efficiency and $<Q_{IR}>$ is the Planck-averaged emissivity at $T = T_{sub}$. Waxman & Draine (2000) studied a similar situation, but for dust surrounding gamma-ray bursts and found that for $2000 < T < 3000$ K, $<Q_{IR}> \approx 0.1$ for a mixture of astronomical silicate and graphite grains with typical sizes of $0.1 \mu\text{m}$. Sollerman et al. (2004) have estimated the peak bolometric luminosity of SN Ia to be $L_{bol} = 1.43 \cdot M_{Ni} \cdot 10^{43} \text{ ergs/s}$, where the ^{56}Ni mass (in units of solar masses), M_{Ni} , has been measured to be between 0.1 and $1.1 M_\odot$ (Leibundgut 2000). Inserting this peak luminosity ($E_\gamma \sim 1 - 5 \text{ eV}$) into Eq. (1), and assuming that all the radiation is absorbed, we find $r_c \lesssim 10^{16} \text{ cm}$ ($\sim 0.003 \text{ pc}$), which we will use as a rough estimate of the region where evaporation of pre-existing dust would take place as a result of the SN heating. A similar estimate of the region that ought to be depleted of dust was done by Pearce & Mayes (1986). Thus, to create a dust shell that would survive the radiation from the supernova explosion, and using the stellar wind velocities and mass-loss rates from Section 2, the wind must start about 10–100 years prior to the explosion, i.e. $\gtrsim 10^{-6} M_\odot$ of mass must be expelled for any effect of circumstellar dust to be noticeable. For SN 2005gj, a well-studied example of a supernova with significant interaction with the circumstellar environment, Aldering et al. (2006) find evidence for mass-loss about 8 years before the explosion. For significant opacity, $\tau \sim 1$, the required dust mass can be estimated from the absorption cross-sections in Weingartner & Draine (2001) and Draine (2003), $\sigma_a/m_{dust} \sim 10^4 \text{ cm}^2/\text{g}$. Thus, for a thin dust shell at $r \sim r_c \sim 10^{16} \text{ cm}$, this corresponds to $m_{dust} \sim 10^{-4} M_\odot$.

We also note that since $r_c \propto \sqrt{M_{Ni}}$, intrinsically brighter explosions are likely to have larger r_c , i.e., thinner circumstellar shells. In the following sections we will see that, depending on the size of the outer shell, multiple scattering could generate relations between brightness and lightcurve shapes and colors qualitatively similar to the observed ranges. We note, however, that interaction with dust in the CS material can only broaden

the pristine lightcurve, i.e., it is not possible to produce a faster decline than what results from the original supernova explosion.

4. MULTIPLE SCATTERING OF PHOTONS AROUND THE SUPERNOVA

A natural effect of light scattering is that it adds flight time to the photons, thereby affecting the observed lightcurve (Patat 2005; Patat et al. 2006). Next, we start by generalizing the Goobar (2008) model: we consider a scenario where the exploding white dwarf ($r_{WD} \sim 10^9 \text{ cm}$) is at the center of a homogeneous dust shell with an outer radius, r ($r \gg r_{WD}$), and an inner radius r_i , where $r_{WD} \leq r_i \leq r$. Note that this will not change any of the results in G08, where $r_i \equiv r_{WD} \approx 0$ was assumed, but it will affect the distribution of photon flight times, i.e., the subject of this paper.

The technique in G08 is extended to investigate the time domain by calculating the total traveled path length, D , for each photon before it crosses a plane, P , that is perpendicular to the line of sight between the observer and the source, and is located at the distance, r , from the source which is illustrated in Fig. A1. The details for the calculation of the photon travel times are outlined in Sec. Appendix A. The traveled photon path length, D , is given by Eq. A1.

The traveled photon path length is distributed in the interval $r \leq D < \infty$, with $D = r$ for photons that do not interact with the dust at all. The shape of the distribution of D will depend on the radius, r , the thickness of the shell, the scattering and absorption properties of the dust, and the dust density. In this work we will quantify the latter in terms of the observed color excess, $E(B-V)$, relative to the pristine source color. For the scattering and absorption properties we use models consisting of carbonaceous grains and amorphous silicate grains from Weingartner & Draine (2001) and Draine (2003).

We begin by exploring the scattering distribution for the two extreme scenarios (a) $r_i = r_{WD} \approx 0$ (i.e., a homogeneous dust sphere as in G08), and (b) $r_i = 0.95 \cdot r$, i.e., a very thin dust shell. Clearly, the scenario (a) is already challenged by the conclusions in Section 3, nevertheless, it serves as a point of reference. The left panel of Fig. 1 shows the distribution of D/r from Monte Carlo simulations of photons with $\lambda = 5000 \text{ \AA}$. Most photons travel unscattered, and for the rest, there is a rough exponential fall-off of delay times. The dust density was chosen to cause an observed color excess $E(B-V) \approx 0.5$. Furthermore, we are assuming that the dust grain properties correspond to LMC-type dust, although the time distributions for MW-type dust are very similar.

A local minimum can be noted for case (b) around $D/r \sim 2$. This can be understood by realizing that photons from the source can only double the path length, $D/r \sim 2$, by having a total scattering angle of $\sim \pi/2$ for this particular setup, which will take it through more dust than for other angles. It is then likely to scatter again, which would result in either a shorter or a longer path. The significance of the minimum will decrease with the density of the dust and the inner radius of the shell.

5. LIGHTCURVE PERTURBATION FROM MULTIPLE SCATTERING

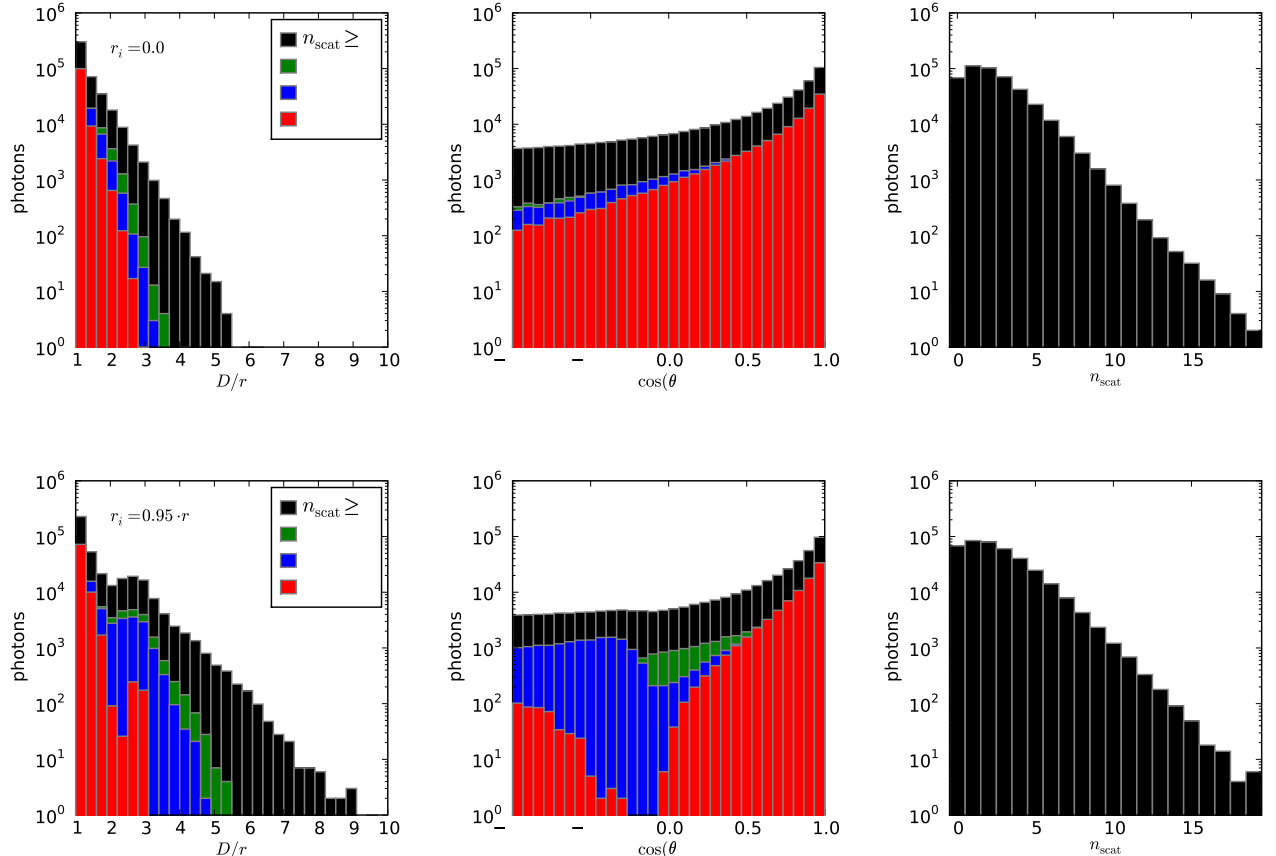


Figure 1. Monte Carlo results of two extreme circum stellar dust scenarios with a dust density corresponding to an observed $E(B - V) = 0.5$. The *upper* and *lower* panels show the results for $r_i = 0.0$ and $r_i = 0.95 \cdot r$ respectively. The *left* panels show the histograms of the total traveled photon paths D (see Sec. Appendix A for definition) normalized with the radius, R , of the sphere, while the *middle* panels show the histogram of the total scattering angles, and the *right* panels show the number of scatters. The local minimum around $D/r \sim 2$ for the lower left panel is related to the lack of photons in the lower middle panel around $\cos(\theta_{\text{tot}}) \sim 0$ with $n_{\text{scat}} = 1$.

Since the scattering cross-section, scattering angle and albedo are wavelength dependent, the lightcurve perturbations are expected to vary between broad-band filters.

We use the time dependent spectral energy distribution (SED) SN Ia templates from Hsiao et al. (2007) (hereafter H07) to build up observed broad-band lightcurves in the presence of circumstellar dust. Thus, we make the simplifying assumption that the empirically derived spectral template is pristine, i.e., not already affected by dust. This is not a major limitation for this analysis, since we are here primarily concerned with relative quantities, such as time-delays or color excess rather than absolute times or fluxes.

Like in G08, we only consider dust grain models from Weingartner & Draine (2001) and Draine (2003) for Milky-Way dust and LMC dust. In particular, it was found in G08 that LMC dust grains in the circumstellar medium would lead to $R_V \approx 1.65$, while Milky-Way dust lead to $R_V \approx 2.56$. These two grain models approximately bracket the empirically found values for R_V for a large fraction of SNe Ia. In both cases, the extinction law deviated significantly from Galactic extinction (Cardelli et al. 1989) in the UV and NIR regions.

For the idealized case considered in this work, a fraction of the photons scatter inside the dust shell and the

delay time induced by the multiple scattering will scale with r ,

$$\Delta t_r \sim \frac{r}{c} \sim 4 \cdot \left(\frac{r}{10^{16} \text{cm}} \right) \text{days}. \quad (2)$$

Since the typical rise-time of SNe Ia lightcurves is about 3 weeks, and the fall-time is somewhat longer, we expect significant effects on the shapes of optical lightcurves for $r \gtrsim 10^{16}$ cm for increasing optical depth, $\tau(\lambda)$. On the other hand, for time scales $\Delta t_r \gg 1$ month, i.e., $r \gg 10^{17}$ cm, we expect the time perturbations to decorrelate with the lightcurve shape perturbations currently used, since these are designed to capture smaller time scale effects.

6. LIGHTCURVE SHAPE

Existing Type Ia supernova lightcurve fitters (Riess et al. 1996; Goldhaber 2001; Wang et al. 2003; Guy 2005; Guy et al. 2007; Jha et al. 2007; Conley et al. 2008; Burns et al. 2011) use different approaches to take variations of the optical lightcurve shape into account for standardizing SNe Ia. To estimate the effect on the lightcurve shape due to circumstellar dust, we once again consider the two extreme scenarios: (a) $r_i = r_{\text{WD}} \approx 0$ and (b) $r_i = 0.95 \cdot r$, introduced above.

Fig. 2 shows the time-delay distribution in the B band

from Monte Carlo simulations as a function of the outer shell radius r for cases (a) and (b) where the LMC-type dust density was chosen to cause an observed color excess $E(B - V) \approx 0.12$.

The far left panel of this figure is closely related to the left panel of Fig. 1, except that the dimensionless property D/r has been converted to days by assuming different physical shell radii. First, we note that for very large outer radii, photons that scatter on dust grains have a fairly flat delay probability with respect to the unscattered ones in the first (zero) bin. We also note how the effect that certain photon paths are less likely for a thin shell, as discussed above, propagates to a sharp feature in the delay time distribution.

Also shown in Fig. 2 is how the delayed photons perturb the pristine B band lightcurve shape. This reveals how the size of the outer radius, affects (primarily) the post-max shape of the lightcurve. Notably, the largest deviation from the pristine shape can be seen in the tail, more than a month after lightcurve maximum, typically beyond the time range investigated for most reddened supernovae.

6.1. The fall-time

The most straight-forward method of quantifying post-maximum lightcurve shape is in terms of the magnitude difference between maximum and an arbitrary number of rest-frame days past maximum in a given rest-frame passband. This method of measuring the fall-time was introduced by Phillips (1993) who chose the rest-frame B band and 15 days past maximum respectively, $\Delta m_{15}(B)$. The simulation results of the evolution of the $\Delta m_{15}(B)$ parameter for a few different CS-scenarios is presented in the far right panel of Fig. 2 and in more detail in Fig. 3.

For $10^{16} \lesssim r \lesssim 5 \cdot 10^{17}$ cm, $\Delta m_{15}(B)$ decreases with r . However, for larger radii, the late photons populate the tail of the lightcurve, i.e., and thus the original pristine lightcurve fall-time at earlier epochs is gradually recuperated, while a plateau is built up at late times. The significance and the variation of the lightcurve tails in the examples shown suggests further studies of the fall-time, also at epochs beyond day 15. This is illustrated by the right panel of Fig. 3, where two different radii for the same dust configuration can give rise to the same value of $\Delta m_{15}(B)$, but different values at 35 days past maximum, $\Delta m_{35}(B)$. For very large radii, both the original values $\Delta m_{15}(B)$ and $\Delta m_{35}(B)$ are recovered. For these extreme radii, the imprint from the CS dust will be found for even later epochs.

Another interesting effect occurs for the dust shell scenario (b) as shown in Fig. 2. The fall-off of the $r = 10^{18}$ cm curve is initially steeper than the $r = 10^{17}$ cm curve, but at day ~ 30 past maximum, this changes and the $r = 10^{18}$ cm curve flattens out and cross the $r = 10^{17}$ cm curve, while the latter continues to fall. This qualitative behavior can also be seen in real data: two SNe Ia normalized to the same maximum brightness show different relative fall-off for different epochs, as seen in Fig. 4.

6.2. The rise-time – fall-time relation

The impact of the time-delay effect from scattering on CS material is expected to have a stronger impact on the

fall-time than on the rise-time of the lightcurve. The relation between the SNe Ia rise time and $\Delta m_{15}(B)$ has been studied both for high-quality data of well-sampled nearby SNe Ia (Strovink 2007), as well as in a statistical approach for a much larger SDSS-II data set (Hayden et al. 2010). While Strovink (2007) found double-peaked distribution for the relation between rise and fall time, this was not seen by (Hayden et al. 2010). Fig. 2 reveals that different CS-dust scenarios could give rise to a relation between rise and fall time, even when a single pristine light source is assumed. In Fig. 5 we show this relation for a few different scenarios, together with the results from Strovink (2007).

The absolute values of any lightcurve parameters determined from our simulations will depend on the corresponding values of the pristine source. Since the lightcurve parameters of the H07 template will roughly reflect the mean values of the SN Ia population, our simulations will only be able to produce lightcurves with longer rise times and smaller $\Delta m_{15}(B)$ than average. In the CS scenario it is reasonable to assume that a “naked” SN Ia template have shorter generic rise time and a faster fall-time, in order to compensate for this we have also applied an add-hoc shift to all curves in Fig. 5 in order to match the data points. Further, assuming that the generic B band shape of a “naked” SN Ia is similar to the H07 template that we use here, any modifications to the relative lightcurve properties for different dust scenarios is likely to be of second order, and the general trend and size of the effect should still be valid.

The result from Fig. 5 is that for SNe within a narrow range of observed color excess, CS-dust could naturally give rise to a bi-modal distribution in the relation between rise and fall time for a small sample. However, if the accepted color range is extended, the gap between the two populations will be filled. More generally, it is intriguing that the rise-fall time scatter observed in normal SNe Ia is compatible with our simulations.

6.3. Time of maximum for different wavelengths

Up to this point we have focused on the effect of circumstellar dust on the rest-frame B band, the wavelength range that is traditionally used for doing SN cosmology. Since the scattering and absorption cross-section decreases with wavelength, we expect the delay distribution to affect bluer pass-bands more. One way of studying this is to investigate the impact on the SN rise-time for different filters. However, this is related to comparing the time of maximum in different bands, which is also a property that can be measured quite accurately. Fig. 6 shows the effect on the difference of the time of maximum between the B and the I bands, $t_{\max}^B - t_{\max}^I$, for various CS scenarios. The general trend in the model prediction is that the time between the I band and B band lightcurve maxima increases for slow decliners. Furthermore, the effect is quite sensitive to optical depth, i.e., to the color excess.

7. INTRINSIC COLOR VARIATIONS

G08 explicitly describes both how circumstellar dust reddens the pristine source and derives this reddening law. However, as we have seen due to the time delay, mixing of photons originating from different epochs is expected. Since the delay time, Δt , depends on the shell

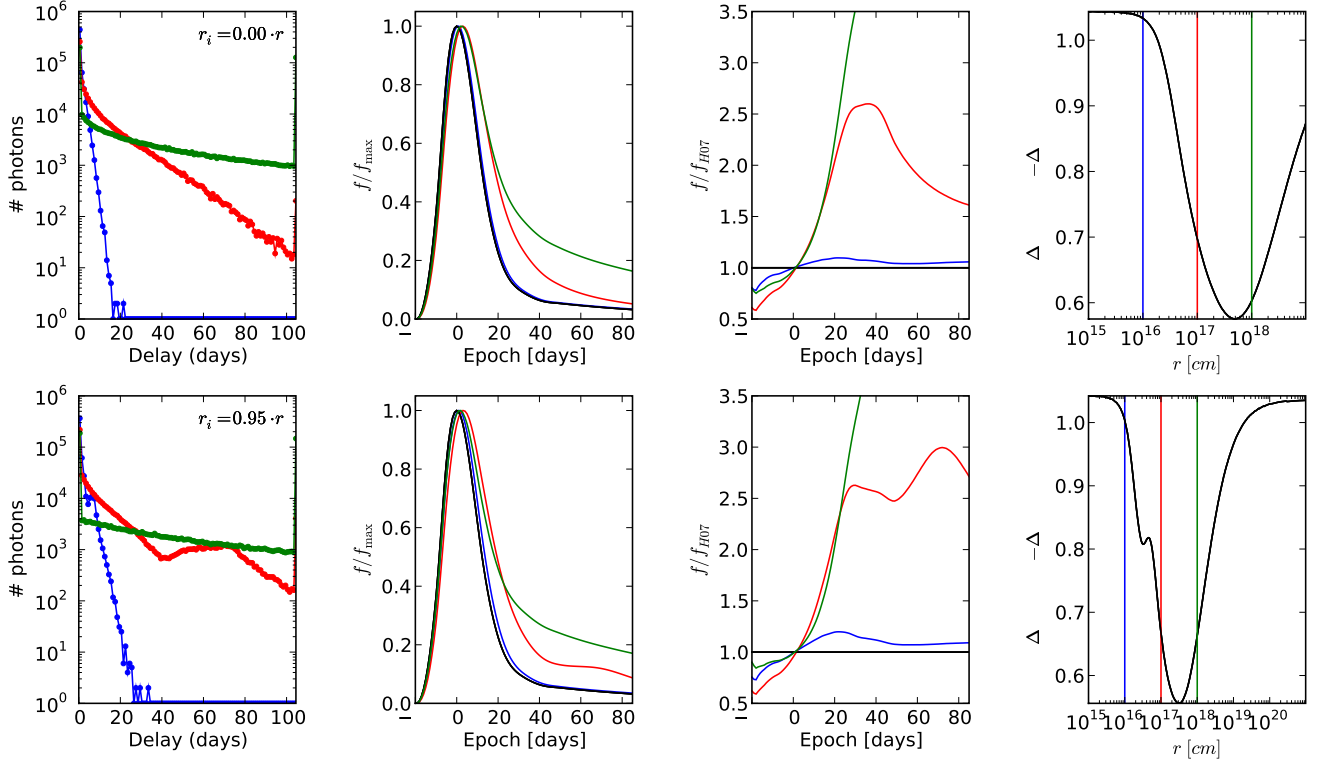


Figure 2. Simulated effects on the SN Ia B band lightcurve from multiple scattering by circumstellar dust for three different radii: (blue, red, green) = ($10^{16}, 10^{17}, 10^{18}$) cm. The *upper* row shows results for $r_i = 0.0$ while the *lower* is for $r_i = 0.95 \cdot r$. A reddening of $E(B - V) \approx 0.12$ has been assumed for both cases. The *far left* column shows the photon delay distribution in the B band. The *middle left* column shows the corresponding B band light curves after the source (black) SED has been convolved by the delay distributions. The *middle right* column gives the B lightcurves normalized by source lightcurve at maximum. The *far right* column shows the B band lightcurve $\Delta_{15}(B)$ for different values of circum stellar shell radii.

radius, the observed color for a fixed dust amount will have an intrinsic scatter with a magnitude depending on the distribution of the shell size, r .

Fig. 7 shows how a few different CS-scenarios could affect both the lightcurve shape and the color at B band maximum. As with previous results we can see that the effects of both lightcurve shape and color increases with the amount of CS-dust. There is also degeneracy between different CS scenarios, so no trivial correlation between fall-time and color excess is expected in the CS-scenario. The CS-model thus naturally accommodates an intrinsic color scatter in moderately reddened supernovae, $\sigma_{E(B-V)} \sim 0.05 - 0.1$ mag, in agreement with observations (Nobili & Goobar 2008; Kessler et al. 2010).

7.1. Time dependent color excess

One of the salient features of the scenario in G08 is that blue photons scatter more than red photons. This implies that blue photons will, on average, be more delayed by multiple scattering since they have a longer path-length before leaving the circumstellar dust environment. This implies that the color excess due to the dust component will acquire time dependence. With respect to a time averaged color excess, the measured color will be redder pre-max turning bluer after max, as shown in Fig. 8. This effect should provide the most stringent bounds on the dust shell sizes allowed by the data. Yamanaka et al. (2009) show in their analysis of SN 2006X that once they

correct for the color excess around maximum light, the $V - R$ color is about 0.3 mag bluer than the normal unreddened SN 2003du 2 months after lightcurve peak, in qualitative agreement with the CS model prediction.

8. PERTURBATIONS TO THE LIGHTCURVE SHAPE-BRIGHTNESS RELATION

Since lightcurve shape is the primary parameter to standardize type Ia supernovae as distance indicators, it is important to investigate how the relation between lightcurve shape and brightness may be affected by the presence of circumstellar dust. As noted in Section 3, an intrinsically brighter explosion will deplete more of the surrounding dust, emphasizing the fainter-redder relation. For shell radii $r \gtrsim 10^{16}$ cm, the optical lightcurve shape will broaden the lightcurves potentially influencing the empirically derived brighter-broader relation. Is it possible to obtain a correlation between brightness and lightcurve shape from the interaction with the circumstellar environment? Although possible, it invokes a somewhat contrived scenario: For shell sizes $r \sim 10^{15} - 5 \cdot 10^{17}$ cm, if the outwards velocity of the circumstellar material, i.e., the white dwarf wind velocity, correlates with the amount of ^{56}Ni powering the explosion, brighter SNe would have large r and become slow decliners. We are not aware of any supernova models that have predictions in this respect.

More generally, if the lightcurve shape is a combination of effects, involving both physics of the progenitor system and the material around the white dwarf, then

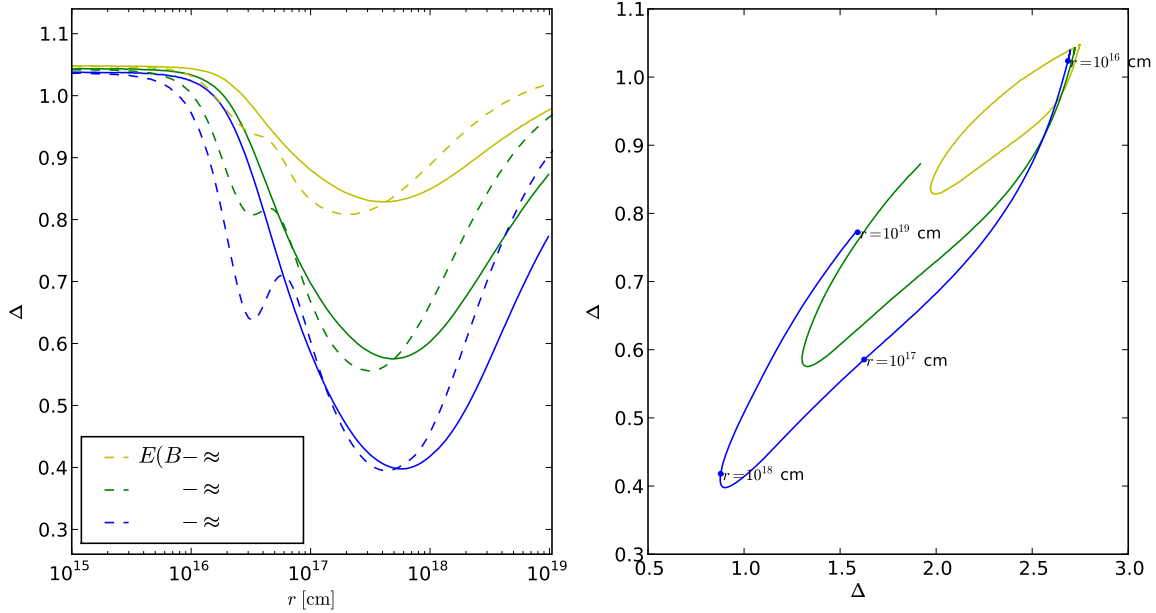


Figure 3. *Left:* evolution of the lightcurve width expressed in terms of $\Delta m_{15}(B)$ for cases (a) (dashed) and (b) (solid) for different amounts of dust. *Right:* the fall time in terms of $\Delta m_{15}(B)$ and $\Delta m_{35}(B)$ as a function of the shell radius.

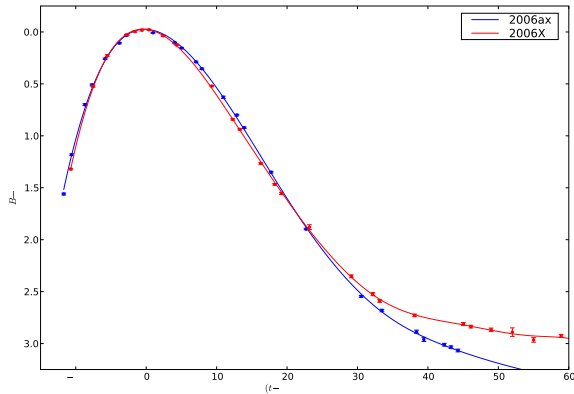


Figure 4. B band lightcurves of 2006ax and 2006X from the Carnegie Supernova Project with $\Delta m_{15}(B) = 0.99$ and $\Delta m_{15}(B) = 1.1$ respectively. The solid lines are smoothed splines. While the fall-off between maximum and day 15 is steeper for 2006X than for 2006ax, this is not true between maximum and for e.g. day 30. The same qualitative appearance can be seen for the CS model in scenario (b) in Fig. 2 if the shell radius is varied.

one would expect a residual dependence of brightness on lightcurve shape, even after the main component has been calibrated out. In particular, we note that the optical lightcurve shape beyond 30 days after B band peak, will be noticeably affected for a wide range of shell sizes.

9. THE SECONDARY “BUMP” IN THE I BAND LIGHTCURVE

The type Ia I band lightcurve exhibits a secondary maximum approximately 15-30 days after the B band lightcurve maximum which, in turn, typically happens within 2 days from the primary I band peak (Nobili et al. 2005). The time gap between the two I band peaks, as well as the relative strength of the secondary peak has

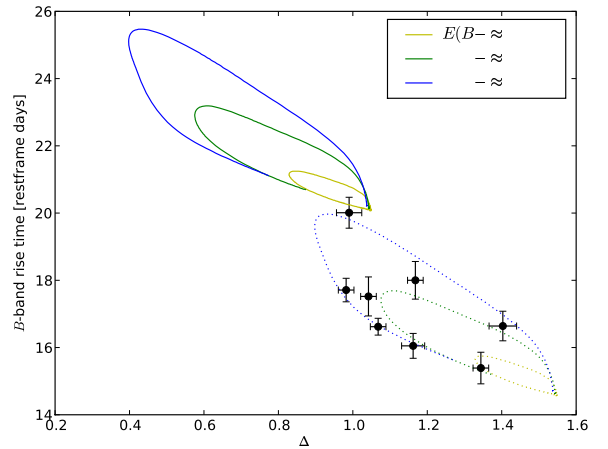


Figure 5. Rise-time vs fall-time imposed by different CS-scenarios. The colors represents different amounts of CS-dust and different points on the individual curves represent varying dust radii. The plot is for a spherical scenario, i.e. $r_i = 0$. Different values on r_i give rise to similar size of the curves, but with slightly different shapes.

been shown to correlate with the B band lightcurve shape (Nobili et al. 2005).

The implication of the imposed time-delay from scattering on circumstellar dust on the I band peaks is shown in Fig. 9. We note that for a constant shell size we expect the brightness difference (upper row) between the peaks, as well as the significance of the secondary peak, to decrease with an increased amount of dust. The effect comes from the fact that photons from the first peak are shifted to both fill the gap between two peaks and emphasize the second bump, and is therefore also correlated with B band fall-time and $E(B-V)$.

If the shell size is allowed to vary, the usual degeneracy

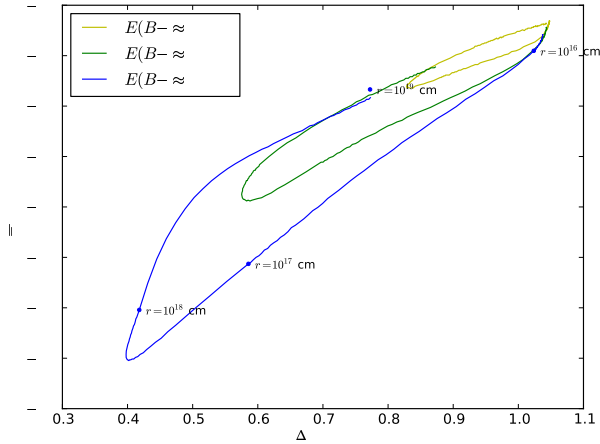


Figure 6. The difference between the time of maximum in the B and I bands for different amounts of CS LMC dust. The curves are shown for a dust sphere, case (a). For the one of the curves, a few different outer radii have been marked for guidance.

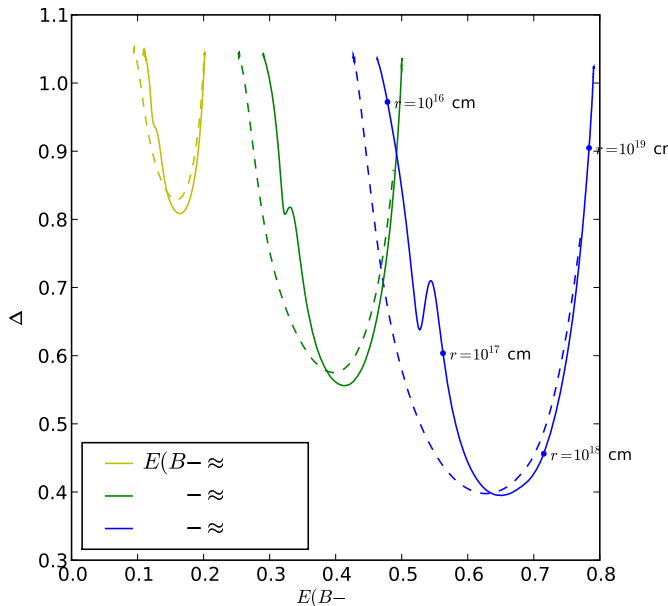


Figure 7. The evolution of $\Delta m_{15}(B)$ and the color excess at B -maximum as a function of the shell radius for cases (a) (dashed) and (b) (solid) respectively.

between shell size and the amount of dust is obtained for the observables. Despite this degeneracy, it is interesting to note that for a broad range of dust properties and shell sizes, a relation between the I band lightcurve properties and $E(B-V)$ is expected.

10. SPECTRAL FEATURES

Folatelli et al. (2010) found that different fitted reddening corrections were obtained for their data set depending on whether the reddest SNe were included in the fit or not. For the full data set they obtained $R_V = 1.7$, while they fitted $R_V = 3.2$ if the high-reddened SNe were excluded. In contrast to this, Amanullah et al. (2010)

found that redder SNe in the Union2 sample prefer a higher color correction than bluer SNe and speculate that the color correction may very well be more complex than a simple linear relation.

Further, Wang et al. (2009) found a bi-modality in the color-magnitude relation over a broad color range, with the two groups preferring different values of R_V independently of the color. They also observed a correlation between the velocity of Si II($\lambda 6355$) and the fitted value of R_V , concluding that objects with high velocity tend to prefer a lower value of R_V than SNe with low velocity.

One possible explanation for the bi-modality could be that the color of the low- R_V SNe primarily originates from CS dust reddening, while the high- R_V objects are dominated by extinction from interstellar dust.

The time-delay of photons from CS dust scattering is expected to blend the spectral energy distributions between different epochs, i.e. a spectral feature for a given epoch will effectively be a superposition of the feature for all previous epochs. Since time-delay distribution varies with wavelength, the amount of blending will also decrease with wavelength. Furthermore, since the minima of the supernova absorption features trace the velocity of the receding photosphere during the first weeks after the explosion, we expect that delayed photons arriving around maximum light will originate from a region further out in the photosphere, i.e., at higher velocities. However, our simulations indicate that these effects are small (see Fig. 10), typically accounting for velocity variations of a few hundred km s^{-1} , i.e., compatible with the velocity scatter between measurements of normal SNe Ia, but not enough to explain significant outliers like SN 2006X (Yamanaka et al. 2009).

11. SUMMARY AND CONCLUSIONS

Dust layers surrounding the progenitor systems of SNe Ia could help explain the observed reddening law. In this work, we have performed Monte Carlo simulations that indicate that the scenario with circumstellar dust would also perturb the supernova optical lightcurves in a manner that resembles empirical findings, e.g., an “intrinsic” color variation of $\sigma_{E(B-V)} \sim 0.05-0.1$ arises naturally in our simulations. Since multiple scattering can only introduce a delay in time, the net effect is a broadening of the lightcurve. While the broadening increases monotonically with the density of dust, the relation with the dust shell size is less straight forward: there is an increase for outer radii about $\sim 10^{17}$ cm, while for even larger radii, the late photons populate the tail instead, and the lightcurve width is closer to the original one. We conclude that well sampled multi-band lightcurves of near-by SNe Ia reaching 2-3 months after lightcurve peak would be critical to probe the existence of dust in the circumstellar environment. Our simulations also suggest that for large optical depths, the lightcurve shape perturbation should be notably different before and after maximum. Furthermore, unlike the case for reddening by interstellar dust, color excess should be epoch dependent: redder earlier on and bluer after maximum.

A strong case for the CS scenario would be if the observed lightcurve perturbations in the optical could be combined with a detection of the emission at longer wavelengths from the heated CS material. A model for this emission was constructed by Dwek (1983) for circum-

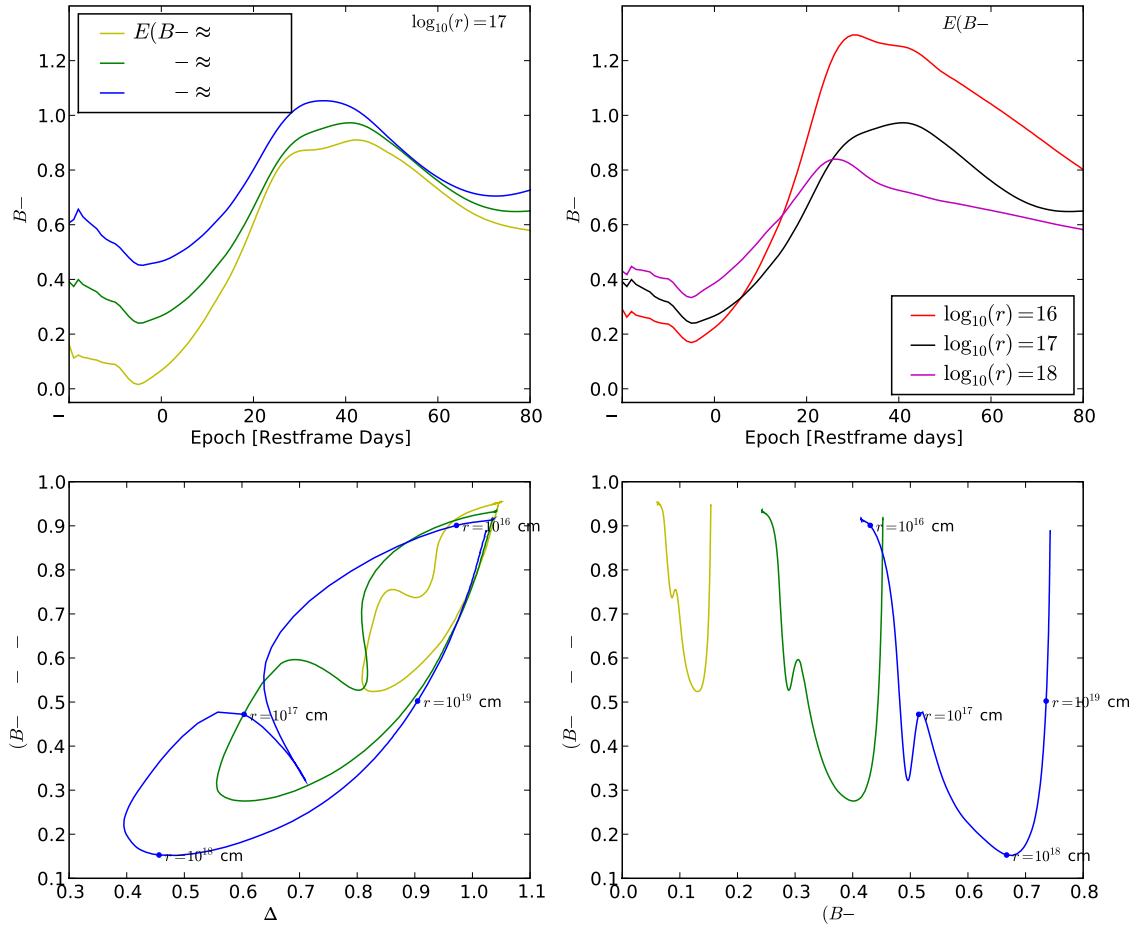


Figure 8. The imposed color for different epochs. The *upper* row shows the $B - V$ color evolution as a function of time, for different amounts of dust (*left*) and different radii (*right*). The lower *lower* row show the color difference between 35 days after B band maximum and maximum brightness for different amounts of LMC dust. This is shown versus the B band fall-time ($\Delta m_{15}(B)$) and the color at maximum in the *left* and *right* columns respectively. The simulated relation between the imposed lightcurve shape, The dust radii for a one of the CS realizations have been plotted along the curve for guidance. All results are shown for a CS scenario (a) with $r_i = 0.95 \cdot r$. The legend describes the color excess the different CS scenarios would give rise to if the time-delay effect on the color is ignored.

stellar dust around Type II SNe. Although the exact properties of the emission is highly model dependent, it is generally expected to last after the optical light has faded.

the Aspen 2010 SN Ia workshop for helpful discussions at the time parts of this manuscript was written. We also acknowledge Adolf Witt for helpful comments on the manuscript.

We are grateful to the organizers and participants of

APPENDIX

A SPHERICAL DUST SHELL

A simple model of a spherical dust-shell with radius, r , and inner radius, $r_i = R \cdot r$, where $0 < R < 1$ is illustrated in Figure A1. Also shown in the figure is a photon leaving the sphere (solid line). The current position of the photon is defined by the vector, $\vec{r}_0 = (x, y, z)$, and the next position, \vec{r}_{next} , is given by $\vec{r}_{\text{next}} = \vec{r}_0 + \vec{r}_D$, where \vec{r}_D is the displacement vector $\vec{r}_D = (dx, dy, dz)$.

Photon traveling inside the shell— The impact parameter, i , is the minimum distance to the center of the sphere for any given photon-path, and can be defined as.

$$i = \begin{cases} r_0 \cdot \sin \gamma & \text{if } 0 \leq \gamma \leq \frac{\pi}{2}, \\ r_0 & \text{if } \frac{\pi}{2} < \gamma. \end{cases}$$

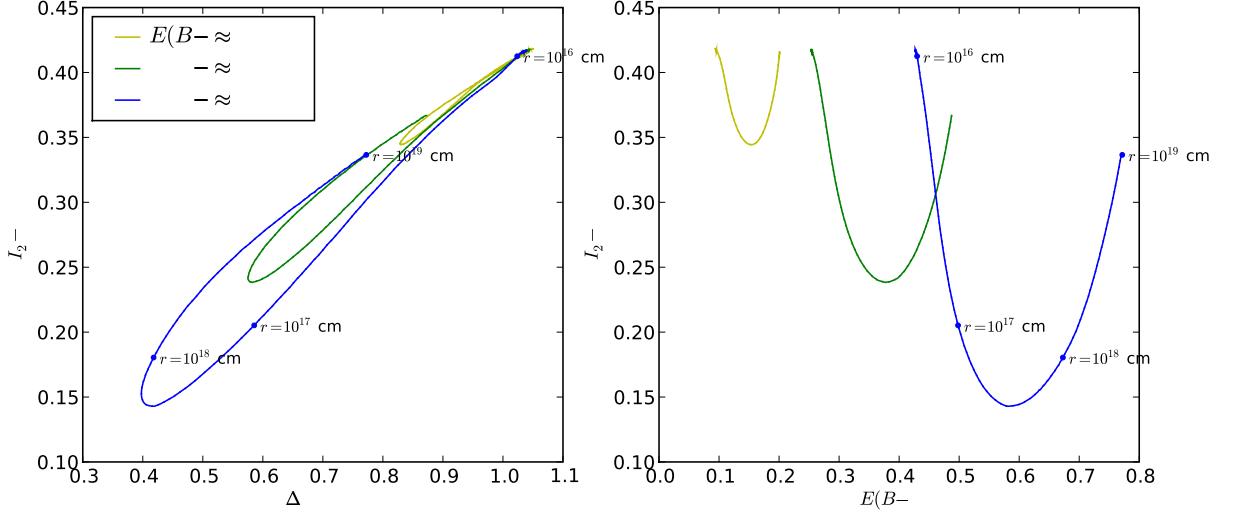


Figure 9. The imposed relation between the extreme points of the I band lightcurve. The difference in brightness between the second and first peak is shown vs the fall-time ($\Delta m_{15}(B)$) and the color excess at B -max ($E(B - V)_0$) respectively. The results are shown for a CS model with $r_i = 0.00 \cdot r$ and LMC-type dust.

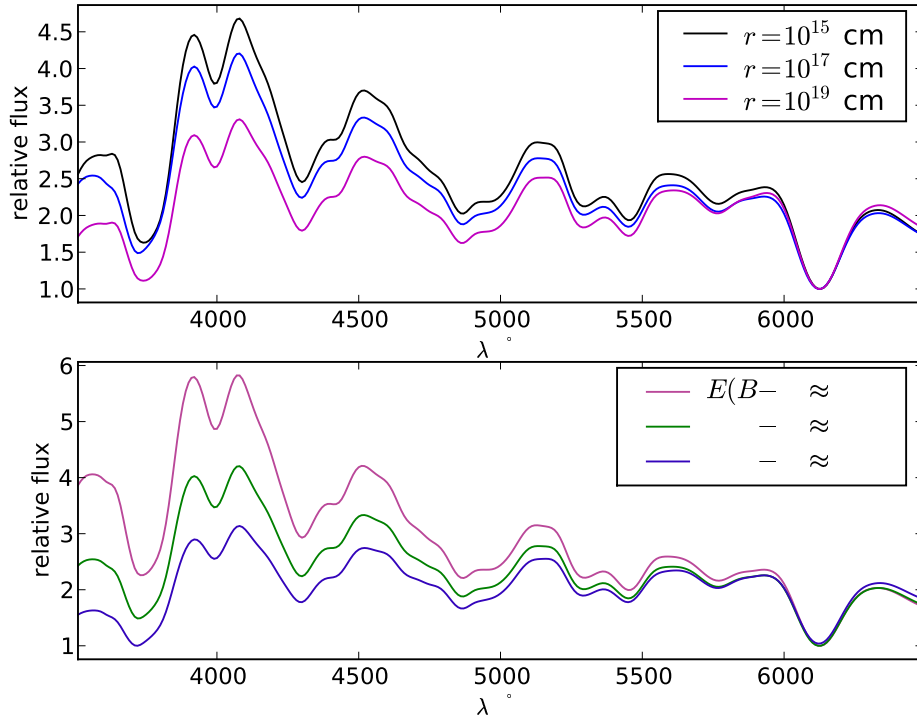


Figure 10. The the impact on the spectrum at maximum from CS dust. The *upper* panel shows the evolution for different shell radii, assuming LMC dust that would give $E(B - V) \approx 0.25$ in the limit when the radius goes to zero. The *lower* panel shows the spectrum for different amounts of dust when the radius is fixed to $r = 10^{17}$ cm. The inner radius is fixed to $r_i = 0.95 \cdot r$ for all cases.

Here, γ is given by

$$\begin{aligned} \bar{r}_0 \cdot \bar{r}_D &= r_0 r_D \cos(\pi - \gamma) = x \cdot dx + y \cdot dy + z \cdot dz \\ \cos \gamma &= -\cos(\pi - \gamma) = -\frac{x \cdot dx + y \cdot dy + z \cdot dz}{r_0 r_D}. \end{aligned}$$

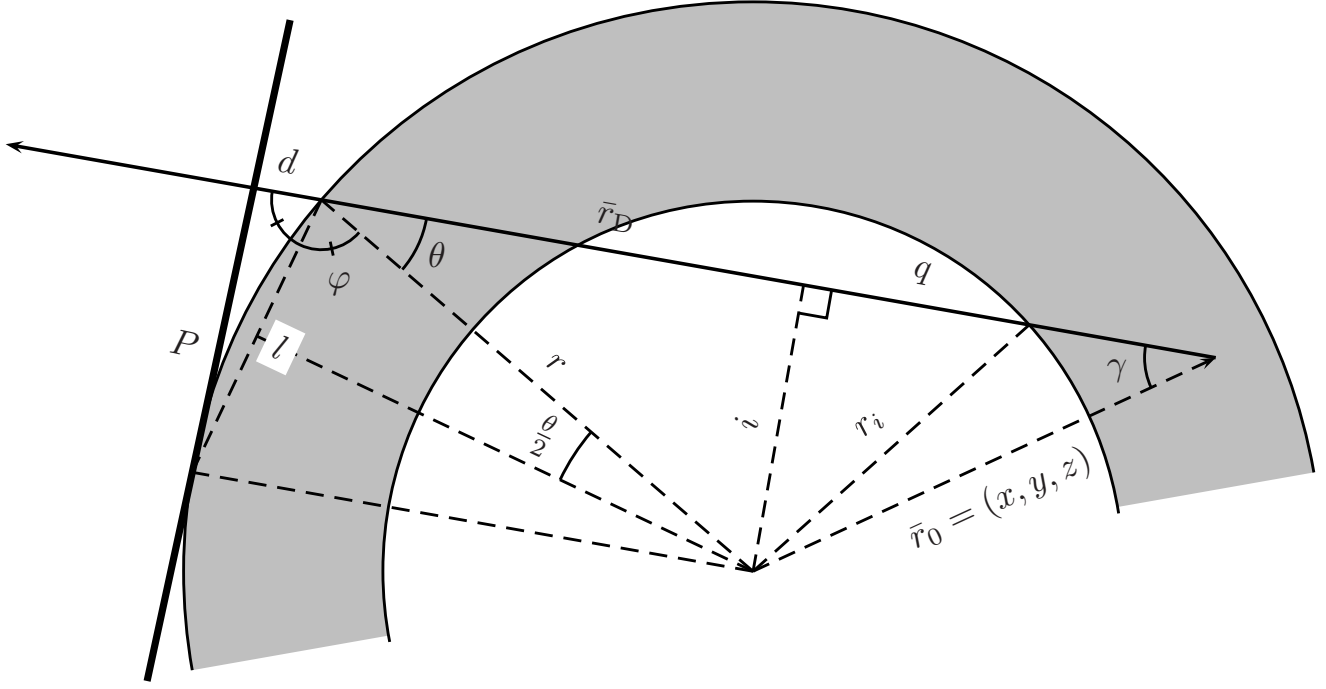


Figure A1. Illustration of a scattered photon (*thin solid line*) propagating through dust shell. The figure shows the intersecting plane of the sphere that is defined by the two vectors \bar{r}_0 and \bar{r}_D .

If $i < r_i$, the photon will cross the inner radius of the shell and then re-enter the shell. This will in turn extend the mean free path of the photon by the amount $2q = 2\sqrt{r_i^2 + i^2}$, which is the length of the path within r_i .

Path length— For each distance between interactions, r_D is added to the total distance traveled by the photon before leaving the sphere. For a scattered photon leaving the sphere, the last distance, s , traveled inside the sphere is given by

$$s^2 = r^2 + r_0^2 - 2rr_0 \cos(\pi - \theta - \gamma),$$

where $\cos \theta = \sin \gamma \cdot r_0 / r$. The distance traveled by a scattered photon should be compared to the distance traveled by a non-interacting photon, which means that the distance, d , between the surface of the sphere and the plane (thick, solid line in Figure A1) perpendicular to \bar{r}_D at distance r from the center must be added to the total distance, where d is given by

$$\begin{aligned} l &= 2r \cdot \sin \frac{\theta}{2} \\ \varphi &= \pi - \frac{\pi}{2} - \frac{\theta}{2} = \frac{\pi - \theta}{2} \\ d &= l \cdot \cos \varphi = 2r \cdot \sin \frac{\theta}{2} \cos \frac{\pi - \theta}{2} = 2r \cdot \sin^2 \frac{\theta}{2}. \end{aligned}$$

The total distance traveled, D , can then be summarized as

$$D = \begin{cases} r & \text{for non-interacting photons,} \\ \sum r_{Dn} + s + d & \text{for scattered photons.} \end{cases} \quad (\text{A1})$$

REFERENCES

- Aldering, G., et al. 2006, ApJ, 650, 510
Amanullah, R., et al. 2010, ApJ, 716, 712
Astier, P., et al. 2006, A&A, 447, 31
Burns, C. R., et al. 2011, AJ, 141, 19
Cardelli, J. A., Clayton, G. C., & Mathis, J. S. 1989, ApJ, 345, 245
Conley, A., et al. 2008, ApJ, 681, 482
Draine, B. T. 2003, ApJ, 598, 1017
Dwek, E. 1983, ApJ, 274, 175
Elias-Rosa, N., et al. 2006, MNRAS, 369, 1880
Elias-Rosa, N., et al. 2008, MNRAS, 384, 107

- Folatelli, G., et al. 2010, AJ, 139, 120
- Goldhaber, G. e. a. 2001, ApJ, 558, 359
- Goobar, A. 2008, ApJ, 686, L103
- Guy, J., et al. 2007, A&A, 466, 11
- Guy, J. e. a. 2005, A&A, 443, 781
- Hachisu, I., & Kato, M. 1999, ApJ, 517, L47
- Hachisu, I., Kato, M., & Nomoto, K. 1996, ApJ, 470, L97+
- Hachisu, I., Kato, M., Nomoto, K., & Umeda, H. 1999, ApJ, 519, 314
- Hamuy, M., Phillips, M. M., Suntzeff, N. B., Schommer, R. A., Maza, J., Smith, R. C., Lira, P., & Aviles, R. 1996, AJ, 112, 2438
- Hayden, B. T., et al. 2010, ApJ, 712, 350
- Hsiao, E. Y., Conley, A., Howell, D. A., Sullivan, M., Pritchett, C. J., Carlberg, R. G., Nugent, P. E., & Phillips, M. M. 2007, ApJ, 663, 1187
- Jha, S., Riess, A. G., & Kirshner, R. P. 2007, ApJ, 659, 122
- Kessler, R., et al. 2009, ApJS, 185, 32
- Kessler, R., et al. 2010, ApJ, 717, 40
- Kowalski, M., et al. 2008, ApJ, 686, 749
- Krisciunas, K., et al. 2007, AJ, 133, 58
- Leibundgut, B. 2000, A&A Rev., 10, 179
- Nobili, S., et al. 2005, A&A, 437, 789
- Nobili, S., & Goobar, A. 2008, A&A, 487, 19
- Nordin, J., Goobar, A., & Jönsson, J. 2008, JCAP, 2, 8
- Patat, F. 2005, MNRAS, 357, 1161
- Patat, F., Benetti, S., Cappellaro, E., & Turatto, M. 2006, MNRAS, 369, 1949
- Pearce, G., & Mayes, A. J. 1986, A&A, 155, 291
- Perlmutter, S., et al. 1999, ApJ, 517, 565
- Perlmutter, S. e. a. 1997, Bulletin of the American Astronomical Society, 29, 1351
- Phillips, M. M. 1993, ApJ, 413, L105
- Riess, A. G., et al. 1998, AJ, 116, 1009
- Riess, A. G., Press, W. H., & Kirshner, R. P. 1996, ApJ, 473, 88
- Riess, A. G., et al. 2007, ApJ, 659, 98
- Sollerman, J., et al. 2004, A&A, 428, 555
- Strovink, M. 2007, ApJ, 671, 1084
- Wang, L. 2005, ApJ, 635, L33
- Wang, L., Goldhaber, G., Aldering, G., & Perlmutter, S. 2003, ApJ, 590, 944
- Wang, X., et al. 2009, ApJ, 699, L139
- Wang, X., et al. 2008, ApJ, 675, 626
- Waxman, E., & Draine, B. T. 2000, ApJ, 537, 796
- Weingartner, J. C., & Draine, B. T. 2001, ApJ, 548, 296
- Wood-Vasey, W. M., et al. 2007, ApJ, 666, 694
- Yamanaka, M., et al. 2009, PASJ, 61, 713